Formation of 100-nm periodic structures on a titanium surface by exploiting the oxidation and third harmonic generation induced by femtosecond laser pulses

Xian-Feng Li,[1] Cheng-Yun Zhang,[2] Hui Li,[1] Qiao-Feng Dai,[1] Sheng Lan,[1,*] and Shao-Long Tie[3]

[1]*Laboratory of Nanophotonic Functional Materials and Devices, School of Information and Optoelectronic Science and Engineering, South China Normal University, Guangzhou 510006, China*
[2]*School of Physics and Electronic Engineering, Guangzhou University, Guangzhou 510640, China*
[3]*School of Chemistry and Environment, South China Normal University, Guangzhou 510006, China*
[*]*slan@scnu.edu.cn*

Abstract: Periodic surface structures with periods as small as about one-tenth of the irradiating femtosecond (fs) laser light wavelength were created on the surface of a titanium (Ti) foil by exploiting laser-induced oxidation and third harmonic generation (THG). They were achieved by using 100-fs laser pulses with a repetition rate of 1 kHz and a wavelength ranging from 1.4 to 2.2 μm. It was revealed that an extremely thin Ti_xO_y layer was formed on the surface of the Ti foil after irradiating fs laser light with a fluence smaller than the ablation threshold of Ti, leading to a significant enhancement in THG which may exceed the ablation threshold of Ti_xO_y. As compared with Ti, the maximum efficacy factor for Ti_xO_y appears at a larger normalized wavevector in the direction perpendicular to the polarization of the fs laser light. As a result, the THG-dominated laser ablation of Ti_xO_y induces 100-nm periodic structures parallel to the polarization of the fs laser light. The depth of the periodic structures was found to be ~10 nm by atomic force microscopy and the formation of the thin Ti_xO_y layer was verified by energy dispersive X-ray spectroscopy.

OCIS codes: (220.4241) Nanostructure fabrication; (350.3390) Laser materials processing; (190.2620) Harmonic generation and mixing; (160.3900) Metals.

References and links

1. M. Birnbaum, "Semiconductor surface damage produced by ruby lasers," J. Appl. Phys. **36**(11), 3688–3689 (1965).
2. P. M. Fauchet and A. E. Siegman, "Surface ripples on silicon and gallium arsenide under picosecond laser illumination," Appl. Phys. Lett. **40**(9), 824–826 (1982).
3. J. E. Sipe, J. F. Young, J. S. Preston, and H. M. Van Driel, "Laser-induced periodic surface structure. I. Theory," Phys. Rev. B **27**(2), 1141–1154 (1983).
4. J. S. Preston, H. M. Van Driel, and J. E. Sipe, "Pattern formation during laser melting of silicon," Phys. Rev. B Condens. Matter **40**(6), 3942–3954 (1989).
5. S. E. Clark and D. C. Emmony, "Ultraviolet-laser-induced periodic surface structures," Phys. Rev. B Condens. Matter **40**(4), 2031–2041 (1989).
6. J. Wang and C. Guo, "Formation of extraordinarily uniform periodic structures on metals induced by femtosecond laser pulses," J. Appl. Phys. **100**(2), 023511 (2006).
7. J. Bonse, A. Rosenfeld, and J. Krüger, "On the role of surface plasmon polaritons in the formation of laser-induced periodic surface structures upon irradiation of silicon by femtosecond laser pulses," J. Appl. Phys. **106**(10), 104910 (2009).
8. M. Huang, F. Zhao, Y. Cheng, N. Xu, and Z. Xu, "Origin of laser-induced near-subwavelength ripples: interference between surface plasmons and incident laser," ACS Nano **3**(12), 4062–4070 (2009).
9. A. Borowiec and H. K. Haugen, "Subwavelength ripple formation on the surfaces of compound semiconductors irradiated with femtosecond laser pulses," Appl. Phys. Lett. **82**(25), 4462–4464 (2003).

#223871 - $15.00 USD Received 25 Sep 2014; revised 25 Oct 2014; accepted 29 Oct 2014; published 5 Nov 2014

10. R. Le Harzic, H. Schuck, D. Sauer, T. Anhut, I. Riemann, and K. König, "Sub-100 nm nanostructuring of silicon by ultrashort laser pulses," Opt. Express **13**(17), 6651–6656 (2005).
11. D. Dufft, A. Rosenfeld, S. K. Das, R. Grunwald, and J. Bonse, "Femtosecond laser-induced periodic surface structures revisited: a comparative study on ZnO," J. Appl. Phys. **105**(3), 034908 (2009).
12. L. Qi, K. Nishii, and Y. Namba, "Regular subwavelength surface structures induced by femtosecond laser pulses on stainless steel," Opt. Lett. **34**(12), 1846–1848 (2009).
13. X. Jia, T. Q. Jia, Y. Zhang, P. X. Xiong, D. H. Feng, Z. R. Sun, J. R. Qiu, and Z. Z. Xu, "Periodic nanoripples in the surface and subsurface layers in ZnO irradiated by femtosecond laser pulses," Opt. Lett. **35**(8), 1248–1250 (2010).
14. J. F. Young, J. S. Preston, H. M. van Driel, and J. E. Sipe, "Laser-induced periodic surface structures. II. Experiments on Ge, Si, Al, and brass," Phys. Rev. B **27**(2), 1155–1172 (1983).
15. F. Costache, M. Henyk, and J. Reif, "Modification of dielectric surfaces with ultra-short laser pulses," Appl. Surf. Sci. **186**(1-4), 352–357 (2002).
16. T. Q. Jia, H. X. Chen, M. Huang, F. L. Zhao, J. R. Qiu, R. X. Li, Z. Z. Xu, X. K. He, J. Zhang, and H. Kuroda, "Formation of nanogratings on the surface of a ZnSe crystal irradiated by femtosecond laser pulses," Phys. Rev. B **72**(12), 125429 (2005).
17. R. Le Harzic, D. Dörr, D. Sauer, F. Stracke, and H. Zimmermann, "Generation of high spatial frequency ripples on silicon under ultrashort laser pulses irradiation," Appl. Phys. Lett. **98**(21), 211905 (2011).
18. G. Miyaji and K. Miyazaki, "Origin of periodicity in nanostructuring on thin film surfaces ablated with femtosecond laser pulses," Opt. Express **16**(20), 16265–16271 (2008).
19. Y. Dong and P. Molian, "Coulomb explosion-induced formation of highly oriented nanoparticles on thin films of 3C–SiC by the femtosecond pulsed laser," Appl. Phys. Lett. **84**(1), 10–12 (2004).
20. J. W. Yao, C. Y. Zhang, H. Y. Liu, Q. F. Dai, L. J. Wu, S. Lan, A. V. Gopal, V. A. Trofimov, and T. M. Lysak, "High spatial frequency periodic structures induced on metal surface by femtosecond laser pulses," Opt. Express **20**(2), 905–911 (2012).
21. A. Y. Vorobyev, A. N. Topkov, O. V. Gurin, V. A. Svich, and C. L. Guo, "Enhanced absorption of metals over ultrabroad electromagnetic spectrum," Appl. Phys. Lett. **95**(12), 121106 (2009).
22. J. Bonse, S. Höhm, A. Rosenfeld, and J. Krüger, "Sub-100-nm laser-induced periodic surface structures upon irradiation of titanium by Ti:sapphire femtosecond laser pulses in air," Appl. Phys., A Mater. Sci. Process. **110**(3), 547–551 (2013).
23. J. Bonse, J. Krüger, S. Höhm, and A. Rosenfeld, "Femtosecond laser-induced periodic surface structures," J. Laser Appl. **24**(4), 042006 (2012).
24. S. K. Das, A. Rosenfeld, M. Bock, A. Pfuch, W. Seeber, and R. Grunwald, "Scattering-controlled femtosecond-laser induced nanostructuring of TiO_2 thin films," Proc. SPIE **7925**, 79251B (2011).
25. S. K. Das, C. Schwanke, A. Pfuch, W. Seeber, M. Bock, G. Steinmeyer, T. Elsaesser, and R. Grunwald, "Highly efficient THG in TiO_2 nanolayers for third-order pulse characterization," Opt. Express **19**(18), 16985–16995 (2011).
26. A. Borowiec and H. K. Haugen, "Subwavelength ripple formation on the surfaces of compound semiconductors irradiated with femtosecond laser pulses," Appl. Phys. Lett. **82**(25), 4462–4464 (2003).
27. A. A. Ionin, S. I. Kudryashov, S. V. Makarov, L. V. Seleznev, D. V. Sinitsyn, A. E. Ligachev, E. V. Golosov, and Yu. R. Kolobov, "Sub-100 nanometer transverse gratings written by femtosecond laser pulses on a titanium surface," Laser Phys. Lett. **10**(5), 056004 (2013).
28. E. V. Golosov, A. A. Ionin, Yu. R. Kolobov, S. I. Kudryashov, A. E. Ligachev, Yu. N. Novoselov, L. V. Seleznev, and D. V. Sinitsyn, "Ultrafast changes in the optical properties of a titanium surface and femtosecond laser writing of one-dimensional quasi-periodic nanogratings of its relief," Sov. Phys. JETP **113**(1), 14–26 (2011).
29. E. V. Golosov, V. I. Emel'yanov, A. A. Ionin, Yu. R. Kolobov, S. I. Kudryashov, A. E. Ligachev, Yu. N. Novoselov, L. V. Seleznev, and D. V. Sinitsyn, "Femtosecond laser writing of subwave one-dimensional quasiperiodic nanostructures on a titanium surface," JETP Lett. **90**(2), 107–110 (2009).
30. N. I. Zheludev, P. J. Bennett, H. Loh, S. V. Popov, I. R. Shatwell, Y. P. Svirko, V. E. Gusev, V. F. Kamalov, and E. V. Slobodchikov, "Cubic optical nonlinearity of free electrons in bulk gold," Opt. Lett. **20**(12), 1368–1370 (1995).
31. P. J. Bennett, A. Malinowski, B. D. Rainford, I. R. Shatwell, Y. P. Svirko, and N. I. Zheludev, "Femtosecond pulse duration measurements utilizing an ultrafast nonlinearity of nickel," Opt. Commun. **147**(1–3), 148–152 (1998).
32. J. Bonse, H. Sturm, D. Schmidt, and W. Kautek, "Chemical, morphological and accumulation phenomena in ultrashort-pulse laser ablation of TiN in air," Appl. Phys., A Mater. Sci. Process. **71**(6), 657–665 (2000).
33. H. Long, A. Chen, G. Yang, Y. Li, and P. Lu, "Third-order optical nonlinearities in anatase and rutile TiO_2 thin films," Thin Solid Films **517**(19), 5601–5604 (2009).
34. K. S. Yee, "Numerical solution of initial boundary value problems involving Maxwell's Equations in isotropic media," IEEE Tran. on Antennas and Propagation **14**, 302–307 (1966). Here, a commercially available software developed by Rsoft Design Group (http://www.rsoftdesign.com) was used for the numerical simulation.
35. SOPRA N&K Database, http://refractiveindex.info/legacy/?group=CRYSTALS&material=TiO2

#223871 - $15.00 USD Received 25 Sep 2014; revised 25 Oct 2014; accepted 29 Oct 2014; published 5 Nov 2014

36. C. Hubert, L. Billot, P.-M. Adam, R. Bachelot, P. Royer, J. Grand, D. Gindre, K. D. Dorkenoo, and A. Fort, "Role of surface plasmon in second harmonic generation from gold nanorods," Appl. Phys. Lett. **90**(18), 181105 (2007).
37. J. Bonse, M. Munz, and H. Sturm, "Structure formation on the surface of indium phosphide irradiated by femtosecond laser pulses," J. Appl. Phys. **97**(1), 013538 (2005).

1. Introduction

Laser-induced periodic surface structures (LIPSSs) created on the surfaces of different materials have been studied for a long time since the appearance of high-power lasers [1–5]. So far, various physical mechanisms have been proposed to interpret the formation of LIPSSs. Early in 1983, it was proposed that LIPSSs originated from the interference between the incident laser light and the surface scattered wave and this mechanism is widely used to explain the formation of LIPSSs on many materials [3]. Recently, it is suggested that the surface plasmon polaritons (SPPs) excited by femtosecond (fs) laser irradiation play a crucial role in the formation of LIPSSs [6–8]. In addition to the conventionally observed LIPSSs with subwavelength periods, LIPSSs with deep subwavelength periods have attracted considerable interest because of their potential applications in the fabrication of functional materials and devices [9–13]. While the LIPSSs with periods approximately equal to the laser wavelength are called low spatial frequency LIPSSs (LSFLs), the LIPSSs with periods much smaller than the laser wavelength are referred to as high spatial frequency LIPSSs (HSFLs). Apparently, HSFLs induced by fs laser pulses cannot be interpreted by using the physical models described above [6–8, 14]. While the orientations of LSFLs are generally perpendicular to the polarization of the laser light, HSFLs with orientations perpendicular or parallel to the polarization of the laser light have been observed. So far, several mechanisms have been proposed to explain the formation of HSFLs induced by fs laser pulses, such as self-organization [15], second harmonic generation (SHG) [9,16,17], excitation of SPPs [18], and Coulomb explosion [19] etc. Recently, we also proposed a mechanism to interpret the formation of HSFLs on the surfaces of some metals such as stainless steel and nickle [20]. In general, laser ablation dominated by SHG is expected to play a crucial role in the formation of HSFLs on the surfaces of semiconductors where SHG is significant [9,16,17]. In comparison, it can be neglected on the surfaces of metals where SHG is not efficient. In order to achieve regular nanostructures with small feature sizes and short periods, laser ablation dominated by high-order harmonic generations is highly desirable and the underlying physical mechanism needs to be investigated.

Titanium (Ti) is a metal which has been widely applied in industry. LIPSSs created on the surface of Ti may significantly alter the physical properties of Ti, leading to some new functions [21]. Both LSFLs and HSFLs were observed in the fs laser ablation of Ti [6,22,23]. In particular, the shortest period of HSFLs was found to be only one-tenth of the irradiation laser wavelength and the physical mechanism responsible for the deep subwavelength period is still under investigation [22–27]. In fact, sub-100-nm HSFLs have been demonstrated in the ablation of Ti by using 790-nm fs laser pulses and it was suggested that laser-induced oxide (i.e., the formation of TiO_2 on the surface of Ti) might play an important role in the formation of such HSFLs [22]. In particular, the authors employed a theoretical model based on the efficacy factor theory proposed by Sipe and associates to interpret the physical origin of the formation of HSFLs. It was mentioned that the linear optical constants cannot satisfactorily describe the formation of HSFLs on Ti surfaces. Apart from laser-induced oxidation, it seems necessary to consider nonlinear optical processes occurring in the ablation of Ti by using fs laser pulses. Another physical mechanism responsible for the sub-100-nm HSFLs formed on Ti surfaces was proposed by Ionin *et al.* They observed sub-100-nm transverse nanoripples on Ti surfaces under multi-shot sub-threshold fs laser irradiation and suggested that such structures were related to frozen patterns of coherent sub-surface nanoscale cavitation [27]. Golosov *et al.* studied the ultrafast changes in the optical properties of a Ti surface during the laser ablation process and found that the dependence of the first-harmonic nanograting

#223871 - $15.00 USD Received 25 Sep 2014; revised 25 Oct 2014; accepted 29 Oct 2014; published 5 Nov 2014

spacing on the laser fluence was determined by the change in the instantaneous optical characteristics of the material and the saturation of the interband absorption along with the increasing role of intraband transitions [28]. Also, they demonstrated that the periods of LIPSSs could be reduced by carrying out the ablation in water with a larger dielectric constant than air [28,29].

In general, bulk metals will not yield any significant third-order nonlinearity owing to free electrons which are expected to have no Kerr-type nonlinearity unless they are confined in microparticles [30]. Similar to most metals that are opaque to the incident laser light, the SHG and THG on the surface of Ti is not efficient in the near infrared spectral region [30,31]. On the other hand, Ti is easily oxidized in air when it is heated to a high temperature, forming titanium oxide Ti_xO_y (such as TiO_2, Ti_2O_3, TiO, and TiO_{2-x}) [22,23,32]. In most cases, the major composition is TiO_2. It has been demonstrated that the efficiency for THG is greatly enhanced once a thin layer of TiO_2 is formed [24,25,33]. Moreover, the maximum efficacy factors for TiO_2 are expected to appear at normalized wavevectors different from those for Ti. As demonstrated in this paper, the maximum efficacy factor for TiO_2 in the direction perpendicular to the polarization of the fs laser light (or THG) appears at a normalized wavevector three times larger than that for Ti. It implies that HSFLs with a period equal to one-third of the THG wavelength can be achieved on Ti_xO_y. This unique feature can be exploited to create HSFLs with small feature sizes and short periods on Ti surfaces.

In this article, we report on the formation of LIPSSs with periods as small as about one-tenth of the irradiating fs laser light wavelength on the surface of a Ti foil by exploiting laser-induced oxidation and THG. It was revealed that an extremely thin Ti_xO_y layer was formed on the surface of the Ti foil after irradiating fs laser light with fluence smaller than the ablation threshold of Ti, leading to a significant enhancement in THG that dominates the subsequent laser ablation process. The depth of the LIPSSs was measured by atomic force microscopy (AFM) while the formation of the thin Ti_xO_y layer was verified by energy dispersive X-ray spectroscopy (EDS) in the scanning electron microscopy (SEM) measurements.

2. Physical model and experimental details

The physical model for creating HSFLs on a Ti foil is schematically shown in Fig. 1. The fs laser light with polarization in the *x* direction is focused on the surface of the Ti foil along the *-z* direction, forming an excitation spot with a diameter of ~40 μm. The laser beam is scanned on the surface of the Ti foil. The laser fluence is intentionally chosen to be lower than the ablation threshold of Ti so that only the oxidation of the surface is induced. Once a thin Ti_xO_y layer is formed, the THG is significantly enhanced and the laser ablation is dominated by the THG. The interference between the THG and the scattered THG will lead to the formation of HSFLs with a period equal to one-third of the THG wavelength on the thin Ti_xO_y layer. Thus, HSFLs with periods equal to about one-tenth of the fs laser wavelength can be obtained on the Ti foil.

In experiments, the HSFLs were produced on the surface of a Ti foil by irradiating fs laser pulses delivered by an optical parametric amplifier (OPerA Solo, Coherent) with wavelengths (λ) ranging from 1.4 to 2.2 μm. The duration and repetition rate of the laser pulses were 100 fs and 1 kHz, respectively. The 0.5-mm-thick Ti foils were purchased from MTI Corporation, China. They were polycrystalline materials with purity of 99% and surface roughness less than 0.5 nm. The laser beam with a diameter of 5.1 mm and a Gaussian profile was focused normally on the surface of the Ti foil by using a lens with a focusing length of f = 150 mm, producing an excitation spot of ~40 μm in diameter (full width at $1/e^2$ of the laser intensity). The laser fluence (F), which is defined as the energy of a single pulse divided by the area of the excitation spot, was adjusted by using the combination of a waveplate and a polarizer. The energy of a single pulse was derived by the average power of the laser pulse train and the repetition rate. The ablation was carried out in air by scanning the laser beam on the surface of the Ti foil. The scanning speed was fixed at 1 mm/s and the average number of laser pulses

#223871 - $15.00 USD Received 25 Sep 2014; revised 25 Oct 2014; accepted 29 Oct 2014; published 5 Nov 2014

irradiating on the excitation spot was estimated to be 40. The morphology of the ablated surface was examined by using both SEM (Ultra55, Zeiss) and AFM (Cypher, Asylum Research). The composition of the formed LIPSSs was examined by EDS with an acceleration voltage of 10 kV, a spatial resolution of ~30 nm and an energy resolution of ~100 eV. The information depth was estimated to be ~590 nm for Ti at an acceleration voltage of 10 kV. The tapping mode was used in the AFM measurements. For the characterization of THG, the fs laser light was incident on the surface of Ti foil at an angle of 45° and the THG was collected in the direction normal to the surface and directed to a spectrometer for analysis.

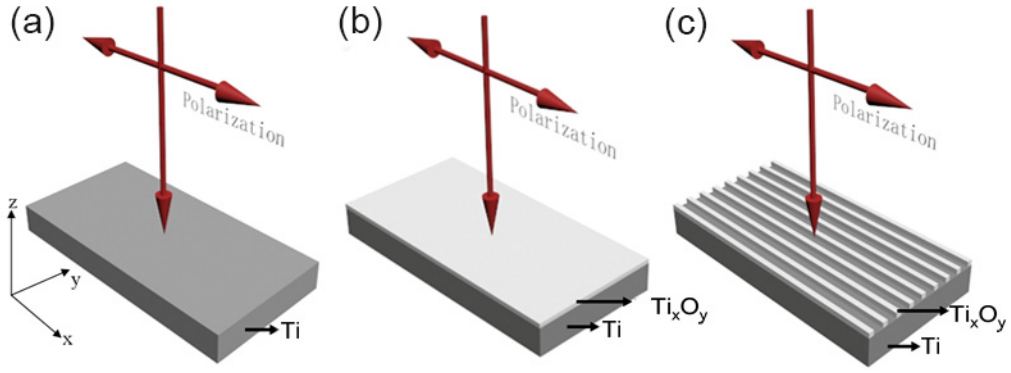

Fig. 1. (a) Surface of a Ti foil irradiated with a fs laser light. (b) Formation of a thin Ti_xO_y layer which enhances significantly THG. (c) Formation of HSFLs with a period equal to one-third of the THG wavelength.

3. Results and discussion

3.1 Morphologies of LIPSSs formed on the surface of a Ti foil

We employed fs laser light with different wavelengths ranging from 1.4 to 2.2 μm to ablate the surface of the Ti foil. The scanning speed of the laser beam was fixed at 1.0 mm/s while the fluence was varied. The morphology of the ablated surface was examined by SEM. For each wavelength, HSFLs with periods ranging from 100 to 140 nm were observed at a critical laser fluence, as shown in Fig. 2. One can see ripples with a width less than 50 nm and an orientation parallel to the polarization of the fs laser light. The critical laser fluences (F) were found to be 0.96, 1.11, 1.27, and 2.23 J/cm^2 for ablation wavelengths of 1.4, 1.8, 2.0, and 2.2 μm. A rapid increase in critical laser fluence was observed at 2.2 μm. It was found that the ablation threshold for long wavelengths (1.4-2.2 μm) were 10-30 times larger than that reported previously for 0.79 μm [22]. This behavior will be discussed later in Section 3.3.

The periods for the HSFLs, which are denoted as Λ, can be easily determined from the Fourier transformations of the SEM images (see the insets of Fig. 3). The periods can be derived from the peak values in the Fourier transformations along the direction perpendicular to the laser polarization, as shown in Fig. 3. They are estimated to be 102, 111, 125, and 140 nm for ablation wavelengths of 1.4, 1.8, 2.0, and 2.2 μm, respectively.

For laser fluences higher than the critical value, the morphology of the ablated surface was changed dramatically, as shown in Fig. 4. LSFLs perpendicular to the polarization of the fs laser light were observed. The periods of the LSFLs are slightly smaller than the wavelength of the fs laser light used for ablation. With increasing ablation wavelength, the period of the LSFLs increases accordingly. This phenomenon is commonly observed in the ablation experiments and it will not be discussed further in this paper.

#223871 - $15.00 USD Received 25 Sep 2014; revised 25 Oct 2014; accepted 29 Oct 2014; published 5 Nov 2014

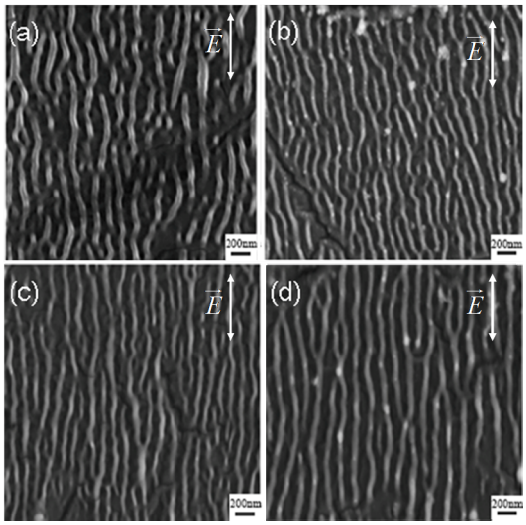

Fig. 2. SEM images showing the formation of HSFLs with periods of ~100-140 nm by using fs laser light with different wavelengths (λ) and fluences (F). (a) λ = 1.4 μm, F = 0.96 J/cm^2; (b) λ = 1.8 μm, F = 1.11 J/cm^2; (c) λ = 2.0 μm, F = 1.27 J/cm^2; (d) λ = 2.2 μm, F = 2.23 J/cm^2. The average number of laser pulses irradiating on the excitation spot was 40. In all cases, the orientation of HSFLs is parallel to the polarization of the fs laser light.

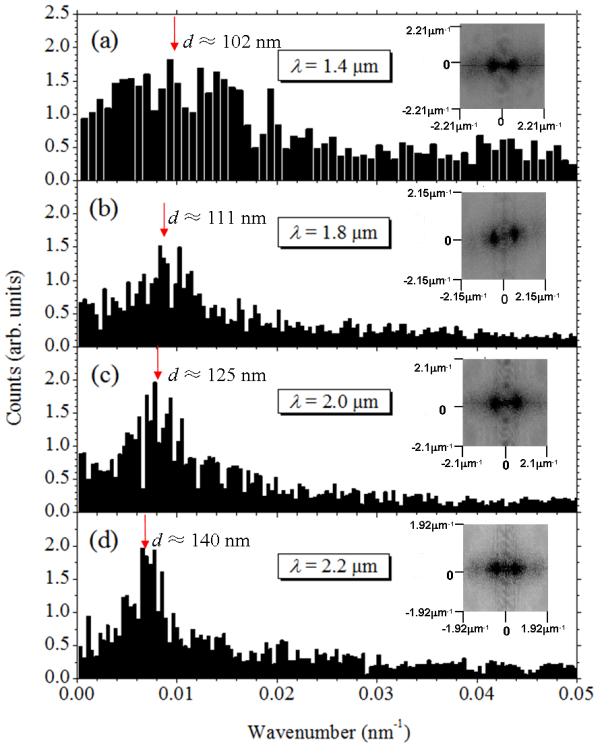

Fig. 3. Fourier transformations of the SEM images for the HSFLs shown in Fig. 2 along the direction perpendicular to the laser polarization for different ablation wavelengths. (a) λ = 1.4 μm, (b) λ = 1.8 μm, (c) λ = 2.0 μm, and (d) λ = 2.2 μm. The insets show the two-dimensional Fourier transformations of the SEM images.

#223871 - $15.00 USD Received 25 Sep 2014; revised 25 Oct 2014; accepted 29 Oct 2014; published 5 Nov 2014

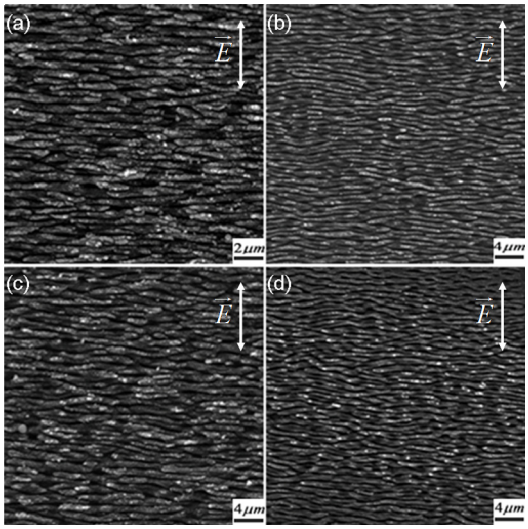

Fig. 4. SEM images showing the formation of LSFLs by using fs laser light with different wavelengths (λ) and fluences (F). (a) λ = 1.4 μm, F = 1.11 J/cm^2; (b) λ = 1.8 μm, F = 1.27 J/cm^2; (c) λ = 2.0 μm, F = 1.59 J/cm^2; (d) λ = 2.2 μm, F = 2.39 J/cm^2. The average number of laser pulses irradiating on the excitation spot was 40. In all cases, the orientation of LSFLs is perpendicular to the polarization of the fs laser light.

From the SEM images, we could only obtain the information on the width and period of the LIPSSs or ripples. In order to know the height or depth of the ripples, we performed AFM measurements on the ablated surfaces and a typical result is shown in Fig. 5(a). From the section graph shown in Fig. 5(b), the height of the ripples or the depth of the grooves is estimated to be ~10 nm.

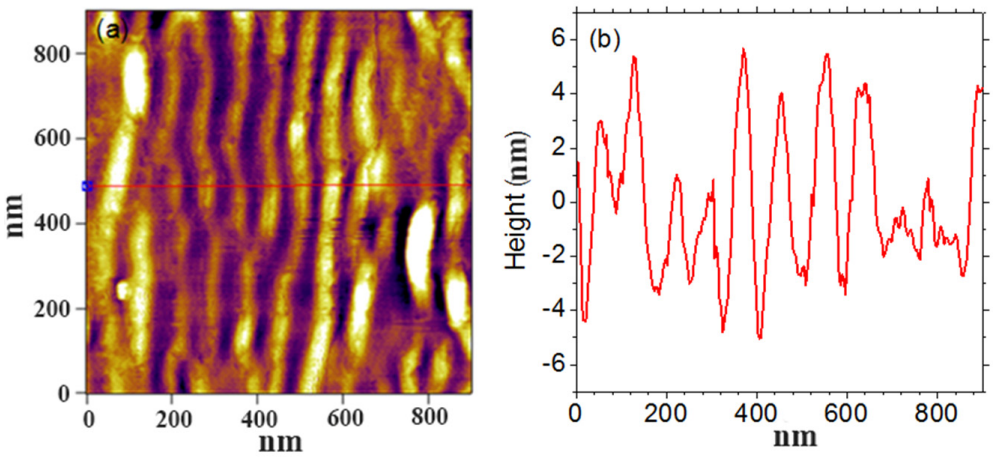

Fig. 5. (a) AFM image for a typical HSFL. (b) Section graph along the straight line in the AFM image showing the height or depth of the HSFL.

3.2 Laser-induced oxidation and enhancement in THG

In the SEM measurements, we employed EDS to examine the composition of the formed HSFLs. The EDS measurements were carried out at an acceleration voltage of 10 kV on both the ridges and the grooves of the HSFLs, as shown in Figs. 6(a) and 6(e). The major elements found in the EDS measurements were C, O, and Ti, as reflected in the EDS spectra shown in

#223871 - $15.00 USD Received 25 Sep 2014; revised 25 Oct 2014; accepted 29 Oct 2014; published 5 Nov 2014

Figs. 6(b) and 6(f). However, a detail analysis of the elements revealed that the content of O in the ridge (17.05%) is much higher than that in the groove (3.42%), implying the formation of a thin Ti_xO_y layer on the Ti surface. It was further confirmed by the line scanning of the K_α signal of O along the straight line perpendicular to the ripples, as shown in Fig. 6(d). A periodic variation of O content was detected and the maxima of the signal appear at the ridges of the HSFLs, as indicated by the arrows. In order to see the influence of the information depth on the measurement results, we also performed the EDS measurements at a higher acceleration of 20 kV and a lower acceleration voltage of 5 kV. When the acceleration voltage was chosen to be 20 kV, the content of O detected in the ridges and grooves of the HSFLs was similar to those observed at 10 kV. When a lower acceleration voltage of 5 kV was used, the K_α and K_β signals of Ti were not excited. We also carried out EDS measurements for a fresh Ti surface and no oxygen was detected, as shown in Fig. 6(h). Although a larger content of O was found in the ridges of the HSFLs, the ratio of O atom to Ti atom at 10 kV is estimated to be 17.05%: 90.54% = 0.19: 1, which is still much smaller than the stoichiometric ratio in TiO_2 which is 2: 1. It indicates the formation of a thin Ti_xO_y layer on the surface of the Ti foil. We think that the major composition of the thin layer is TiO_2 although it may include other compositions such as Ti_2O_3, TiO, and TiO_{2-x}.

As mentioned at the beginning, the formation of a thin Ti_xO_y layer (especially TiO_2 layer) will lead to a significant enhancement in THG [25]. In order to further confirm the laser-induced oxidation of Ti, we irradiated 1.4-μm fs laser light on the surface of the Ti foil at an angle of 45° and detected the SHG/THG signal in the direction normal to the surface. The laser fluence was chosen to be lower than the ablation threshold of Ti. The nonlinear optical response spectra obtained at different excitation intensities are shown in Fig. 7(a). At low excitation intensities, it was found that the intensity of THG was weaker than that of SHG. However, a rapid increase in THG was observed with increasing excitation intensity and it became much stronger than SHG at high excitation intensities.

We also examined the polarization of the THG by placing a polarizer in front of the spectrometer. It was revealed that the polarization of the THG was the same as that of the fs laser light, as shown in Fig. 7(b). When the polarizer was placed to be parallel to the polarization of the fs laser light, the THG could be detected. The THG disappeared completely when the polarizer was changed to be perpendicular to the polarization of the fs laser light. After the THG measurement, we employed EDS to analyze the elements in the area irradiated by the fs laser light. In the EDS measurements, the electron beam was scanned on an area of $1.0 \times 1.0\ \mu m^2$ which was located at the center of the excitation spot. As shown in Fig. 8, a large content of O (23.79%) was detected, confirming the laser-induced oxidation. In contrast, no oxygen was detected in the EDS measurement performed on the Ti surface without irradiation of fs laser pulses. It indicates that the laser-induced thin Ti_xO_y layer can be detected in the EDS measurements while the native oxide layer on the Ti surface is negligible as compared to the laser-induced one. In our case, the content of O measured in the grooves (~3%) is larger than that observed on the non-radiated surfaces, implying that the thickness of the Ti_xO_y layer may be larger than the height of the ripples (~10 nm) determined in the AFM measurements.

#223871 - $15.00 USD Received 25 Sep 2014; revised 25 Oct 2014; accepted 29 Oct 2014; published 5 Nov 2014

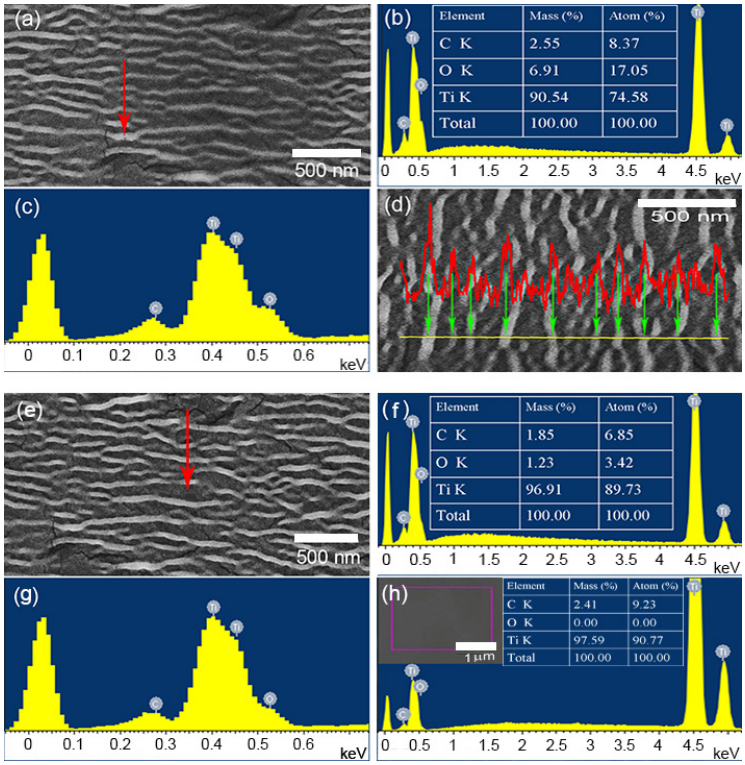

Fig. 6. (a) The SEM image of a selected area of the HSFL in which the EDS measurement was carried out on a ridge of the HSFL, as indicated by the arrow. (b) The EDS spectrum obtained on the ridge of the HSFL as indicated in (a). (c) The enlarged spectrum shown in (b) at the low-energy region. (d) The line scanning of the K_α signal of O showing the periodic variation of the O content along the straight line. The arrows indicate the correspondence between the peaks of the O content and the ridges of the HSFL. (e) The SEM image of a selected area of the HSFL in which the EDS measurement was carried out on a groove of the HSFL, as indicated by the arrow. (f) The EDS spectrum obtained on the groove of the HSFL as indicated in (e). (g) The enlarged spectrum shown in (f) at the low-energy region. (h) The EDS spectrum obtained on a fresh Ti surface with an area of ~2.0 × 1.5 μm^2. The inset shows the SEM image of the Ti surface. The acceleration voltage used in the EDS measurements mentioned above was 10 kV.

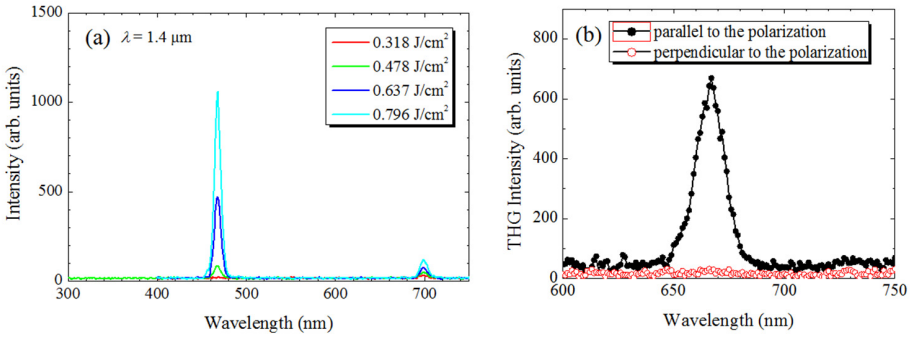

Fig. 7. (a) Nonlinear optical response spectra measured at different excitation intensities. (b) Dependence of the THG intensity on the polarization direction of the polarizer placed in front of the spectrometer. The wavelength of the fs laser light was chosen to be 1.4 μm in both cases.

#223871 - $15.00 USD Received 25 Sep 2014; revised 25 Oct 2014; accepted 29 Oct 2014; published 5 Nov 2014

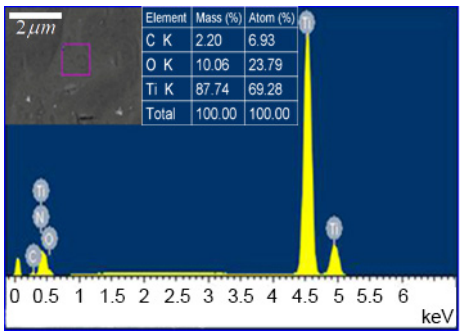

Fig. 8. EDS measurement result obtained on an area of 1.0 × 1.0 μm^2 located at the center of the excitation spot after the THG measurements under laser fluences lower than the ablation threshold. The inset shows the morphology of the central area where the THG measurements were carried out. The square indicates the area on which the EDS measurement was performed.

3.3 Effects of the thin Ti_xO_y layer on the absorption and electric field intensity distribution of fs laser light

Apart from the enhancement in THG, the formation of the thin Ti_xO_y layer may also alter the absorption and intensity distribution of both the fs laser light and the THG which influence the subsequent ablation process. In order to evaluate the effects of the Ti_xO_y layer, we have calculated the evolution of the reflection spectrum with increasing thickness of the TiO_2 layer by using the finite-difference time-domain (FDTD) technique [34], as shown in Fig. 9(a). The software (Fullwave) used for the FDTD simulations was developed by Rsoft Design Guoup. In the numerical simulation, the wavelength dependent complex refractive indexes for Ti and TiO_2 were chosen to be values which are commonly used [35]. In addition, a continuous wave was employed to approximate the pulse train used in the experiments. Since there is no transmission in our case, a decrease in reflection implies an increase in absorption. This behavior is observed at short wavelengths where THG was observed, as indicated by the arrows. It means that the absorption of THG is increased due to the formation of the thin TiO_2 layer, which is helpful for the subsequent ablation of the TiO_2 layer.

In order to gain a deep insight into the ablation of the thin TiO_2 layer, it is necessary to analyze the modification in the electric field intensity distribution of laser light with increasing thickness of the TiO_2 layer at the wavelengths of both the fs laser light and the THG. It can be done by using the FDTD simulations and the results for the fs laser light (1.4 μm) and the THG (0.467 μm) are presented in Figs. 9(b) and 9(c). For the irradiation wavelengths of 1.4 μm and 0.467 μm, the complex refractive indices for Ti were chosen to be 3.8333 + i3.6766 and 1.7233 + i2.3067 while those for TiO_2 were chosen to be 2.5609 + i0 and 2.4815 + i0.7425 [35]. A nonuniform grid was employed in the numerical simulation and the TiO_2 layer was divided into 10 segments in its thickness. Apparently, a strong localization of electric field intensity in the TiO_2 layer is observed and the enhancement in field intensity increases with increasing thickness of the TiO_2 layer. A slight decrease in the electric field intensity is observed near the interface between air and the TiO_2 layer. It originates from the interference between the incident light and the reflected light because we simulate the static electric field intensity distribution. Similar to SHG which is a second-order nonlinear optical process [36], it is expected that the THG intensity is proportional to $\chi^{(3)}(TiO_2) f_1^3(\omega_1) f_2(\omega_2) + \chi^{(3)}(Ti) g_1^3(\omega_1) g_2(\omega_2)$, where $f_1(\omega_1)$ and $f_2(\omega_2)$ represent the electric field intensity enhancement factors (i.e., $|E/E_0|^2$ or I/I_0) for TiO_2 at the wavelengths of the fs laser light and the THG and $g_1(\omega_1)$ and $g_2(\omega_2)$ represent the corresponding values for Ti. As discussed above, the third-order nonlinearity for bulk metals can be neglected because of free electrons. However, the penetration depth of light for metals ranges from several to several tens of nanometers, depending on the conductivity of metals and the wavelength of light. As a result, an

#223871 - $15.00 USD Received 25 Sep 2014; revised 25 Oct 2014; accepted 29 Oct 2014; published 5 Nov 2014

enhancement in $\chi^{(3)}$ is expected due to the skin effect [30]. Considering the large $\chi^{(3)}$ for TiO_2 [25] and the increase of the electric field intensity enhancement factors shown in Figs. 9(b) and 9(c), a significant enhancement in THG intensity is expected with increasing thickness of the TiO_2 layer. It interprets why the thin TiO_2 layer can be easily ablated by the THG. However, it is thought that the THG efficiency is still much smaller when comparing with commercially used crystals such as BBO. It is noticed that the electric field intensity in Ti is also enhanced due to the formation of the TiO_2 layer. The absorption of both the fs laser light and the THG by the Ti beneath the TiO_2 layer will increase the temperature and facilitate the ablation of the TiO_2 layer.

As mentioned in Section 3.1, the ablation thresholds for long-wavelength fs laser light (1.4-2.2 μm) were found to be 10-30 times larger than that reported previously for 0.79 μm [22]. This behavior can be easily understood if we consider the laser-induced oxidation and the THG-dominated ablation. When the wavelength of the fs laser light is chosen at 1.4 μm, the THG appears at 0.467 μm at which the absorption of TiO_2 is small. In comparison, a large absorption is expected at the THG of 0.79 μm (i.e. 0.26 μm) because the absorption of TiO_2 increases rapidly for wavelengths shorter than 0.4 μm. It explains why the ablation threshold becomes much larger for long-wavelength fs laser light. We have measured the ablation threshold for the formation of HSFLs at an ablation wavelength of 2.2 μm. It is about 28 times larger than that reported previously for 0.79 μm [22]. If we consider 0.79 μm as the THG of 2.2 μm, then the THG efficiency is estimated to be 1/28 or 3.6% at the ablation threshold. In experiments, the laser fluence we used at the fundamental wavelength was smaller than the ablation threshold of Ti. The laser energy was partly absorbed by Ti and partly converted to THG. In our case, the thin Ti_xO_y layer was formed on the Ti substrate which would be heated to a high temperature after absorbing the laser energy. Consequently, the temperature rise in the Ti_xO_y layer originated not only from the absorption of THG but also from the temperature rise in the Ti substrate which was induced by the absorption of the fundamental light. In addition, the electric field is found to be strongly localized in the thin Ti_xO_y layer, as shown in Fig. 9. Furthermore, the ablation threshold of a thin Ti_xO_y layer is expected to be lower than that for bulk material. Therefore, a small THG efficiency of ~3.6% can lead to the ablation of the thin Ti_xO_y layer and the formation of the HSFLs, as demonstrated in the experiments.

3.4 Formation of HSFLs parallel to the polarization of the fs laser light on the thin Ti_xO_y layer

So far, the most widely accepted theory used to explain the formation of LIPSSs is the model proposed by Sipe and associates [3], which is based on the interaction of the incident laser beam with a microscopically rough surface. A scalar function $\eta(\boldsymbol{k})$, which is referred to as efficacy factor, is employed to describe the efficiency with which the rough surface absorb the energy of the incident laser beam at the wavevector $|\boldsymbol{k}| = 2\pi/\Lambda$ of the LIPSSs. Based on the model described previously [3,22,37], we can easily calculate the dependence of efficacy factor $\eta(\boldsymbol{\kappa})$ on the normalized wavevector $|\boldsymbol{\kappa}| = \lambda/\Lambda$ for Ti and TiO_2 at both the fundamental wavelength and the THG wavelength.

An example for the fundamental wavelength of 2.0 μm and the THG wavelength of 0.667 μm is presented in Fig. 10. Here, $\kappa_x = \lambda/\Lambda_x$ and $\kappa_y = \lambda/\Lambda_y$ represents the normalized wavevectors and Λ_x and Λ_y denote the periods of the LIPSSs in these directions. The polarization of the incident laser light was along the $\boldsymbol{\kappa}_x$ direction. The parameters used in the calculation include irradiation parameters, material parameters, and surface parameters. For irradiation parameters, the incident angle and the irradiation wavelength were set to be $\theta = 0°$ and $\lambda = 0.667$ or 2.0 μm, respectively. The complex refractive indices used for Ti and TiO_2 were 2.29 + 3.05i and 2.8463 + 0i. The shape factor and the filling factor were chosen to be $s = 0.4$ and $f = 0.1$. As indicated in [22], a narrow sickle-shaped feature with a maximum centered close to $\kappa_x = \pm 1$ ($\kappa_y = 0$) can be seen in Figs. 10(a) and 10(c). It represents LIPSSs

#223871 - $15.00 USD Received 25 Sep 2014; revised 25 Oct 2014; accepted 29 Oct 2014; published 5 Nov 2014

with periods Λ close to the laser wavelength and an orientation perpendicular to the polarization, as shown in Fig. 4.

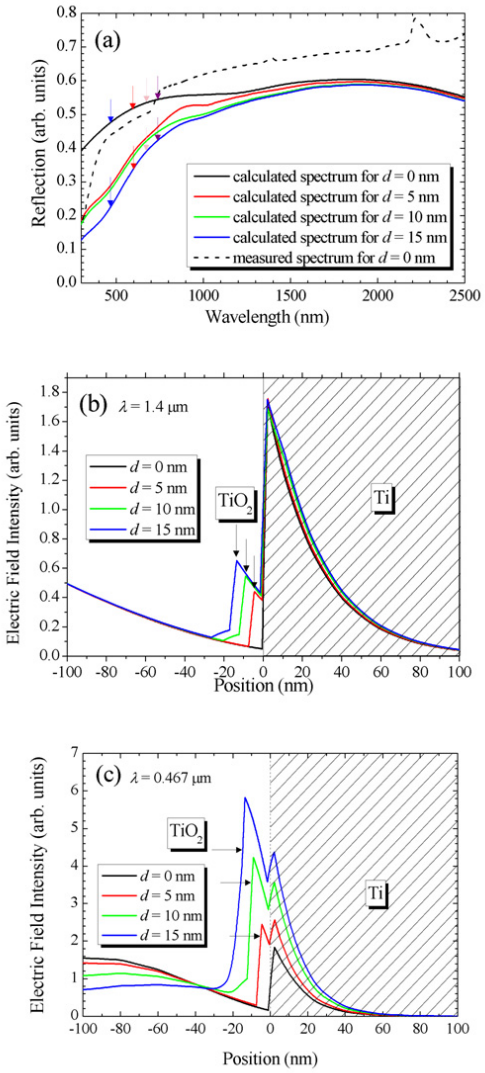

Fig. 9. Evolution of the reflection spectrum (a) and electric filed intensity distribution at the ablation wavelength of 1.4 μm (b) and the THG wavelength of 0.467 μm (c) with increasing thickness of the thin TiO_2 layer. A nonuniform grid was employed in the numerical simulation and the TiO_2 was divided into 10 segments. The arrows in (a) indicate the changes in the reflection at the THG wavelengths when the ablation wavelengths were chosen to be 1.4, 1.8, 2.0, and 2.2 μm.

In order to understand the formation of LIPSSs in the $\boldsymbol{\kappa_x}$ and $\boldsymbol{\kappa_y}$ directions, we present the dependence of η on κ_x (κ_y = 0) and κ_y (κ_x = 0) in Fig. 11. For Ti, it can be seen that the maximum efficacy factor is observed at ± 1.01 in both the $\boldsymbol{\kappa_x}$ and $\boldsymbol{\kappa_y}$ directions regardless of the laser wavelength, implying that only LIPSSs with periods close to the wavelength of the fs laser light or LSFLs can be achieved. It indicates that HSFLs cannot be obtained on the surface of Ti. In comparison, it is noticed that the maximum efficacy factor for TiO_2 appears in the $\boldsymbol{\kappa_y}$ direction at ~ ± 2.86 for λ = 0.667 μm and at ~2.70 for λ = 2.0 μm. It means that

#223871 - $15.00 USD Received 25 Sep 2014; revised 25 Oct 2014; accepted 29 Oct 2014; published 5 Nov 2014

HSFLs with a period equal to about one-third of the laser wavelength can be achieved in this direction and the formed HSFLs are parallel to the laser polarization. Since TiO_2 is almost transparent at λ = 2.0 μm with negligible absorption, the ablation of the thin Ti_xO_y layer is expected to occur at λ = 0.667 μm, as demonstrated in the experiments.

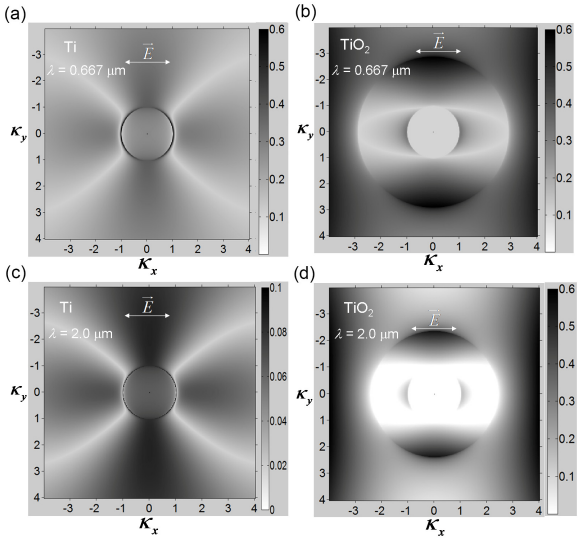

Fig. 10. Dependence of efficacy factor η on normalized wavevector $\boldsymbol{\kappa}$ (κ_x and κ_y) calculated at both the THG wavelength of 0.667 μm for Ti (a) and TiO_2 (b) and the fundamental wavelength of 2.0 μm for Ti (c) and TiO_2 (d) by using the efficacy factor theory [3,22,37].

Owing to the formation of a thin TiO_2 layer, the THG is enhanced significantly [25]. In addition, both the THG and the fundamental laser light are strongly localized in the TiO_2 layer and Ti beneath, leading to an enhancement in the electric field intensity. Consequently, HSFLs with periods equal to about one-tenth of the fs laser light are created when the THG intensity exceeds the ablation threshold of the thin TiO_2 later, which is considered to be much lower than that of bulk TiO_2. Based on the SEM and EDS measurements, we think that the delamination or spallation of the thin Ti_xO_y layer from Ti is a possible mechanism for the formation of HSFLs.

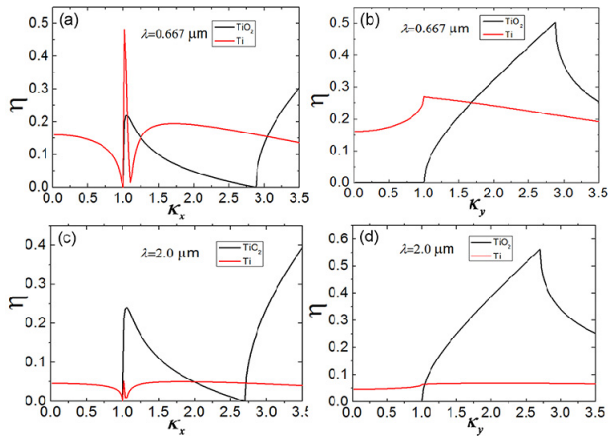

Fig. 11. Dependence of efficacy factor η on normalized wavevector κ_x (κ_y = 0) and κ_y (κ_x = 0) calculated at both the THG wavelength of 0.667 μm ((a) and (b)) and the fundamental wavelength of 2.0 μm ((c) and (d)) for Ti and TiO_2.

#223871 - $15.00 USD Received 25 Sep 2014; revised 25 Oct 2014; accepted 29 Oct 2014; published 5 Nov 2014

In the physical model described above, only the linear absorption of the THG by the thin TiO_2 layer is considered. However, the linear absorption by TiO_2 is significant only for wavelengths shorter than 0.40 μm and the two- or three-photon absorption of the THG needs to be taken into account. Consequently, a larger imaginary part of the complex refractive index is expected for TiO_2. In this case, the peak for TiO_2 appearing in Fig. 11(b) is slightly broadened but its position remains unchanged. Therefore, the consideration of the two- or three photo absorption of the THG does not influence the conclusions drawn in this work. Fortunately, The absorption of both the fs laser light and the THG by the Ti beneath the TiO_2 layer will increase the temperature and facilitate the ablation of the TiO_2 layer.

For the ablation of the thin TiO_2 layer, we employed for simplicity a purely thermal model in combination with the efficacy factor theory to elucidate the formation of the 100-nm HSFLs. In practice, a nonthermal mechanism, such as a multiphoton excitation followed by ultrafast photoionization and Coulomb explosion, is involved in the initial stage of the ablation after the fast excitation. Therefore, there are other competing channels for the conversion of the absorbed energy although we think that the THG process plays a dominant role in the formation of HSFLs. Since these competing channels also contribute to the ablation process, the efficiency for THG given above (~3.6%) is overestimated.

4. Summary

In summary, we have investigated the formation of 100-nm periodic surface structures the surface of a Ti foil. It was revealed that the laser-induced oxidation and enhancement in THG play a crucial role in the creation of such HSFLs. The morphologies of the formed HSFLs were characterized by both SEM and AFM. The periods and depths of the HSFLs were found to be about one-tenth of the fs laser wavelength and about 10 nm. The formation of a thin Ti_xO_y on the surface of the Ti foil was verified by EDS measurements. Also, the modification in the absorption and localization of both the fs laser light and the THG was studied by the numerical simulations based on the FDTD technique. The HSFLs with feature sizes and periods smaller than 100 nm may find applications in the fabrication of functional materials and devices.

Acknowledgments

The authors acknowledge the financial support from the National Natural Science Foundation of China (Grant Nos. 51171066 and 11374109) and the Ministry of Education of China (Grant No. 20114407110002). Q. F. Dai would like to thank the Guangzhou science and technology project (Grant No. 2011J2200080).

#223871 - $15.00 USD Received 25 Sep 2014; revised 25 Oct 2014; accepted 29 Oct 2014; published 5 Nov 2014